Journal of The Electrochemical Society, **154** (11) C684-C691 (2007)
0013-4651/2007/154(11)/C684/8/$20.00 © The Electrochemical Society

The Initial Steps of Atmospheric Corrosion on Magnesium Alloy AZ91D

Martin Jönsson,[z] Dan Persson, and Rolf Gubner

Corrosion and Metals Research Institute (KIMAB), 11428 Stockholm, Sweden

Magnesium, with its low density, is a very interesting metal in applications in which weight is important. In this work the initiation of corrosion attacks on magnesium alloy AZ91D has been investigated under atmospheric conditions, using confocal laser scanning microscopy and SKPFM. The corrosion attack starts in the α phase in larger grains and is under atmospheric conditions initiated at the boundary between the α phase and the eutectic α-/β phase. The SKPFM measurement shows that a high Volta potential difference exists between the larger grains and the surrounding eutectic α-/β phase and the β phase. A microgalvanic element is formed in the thin adlayer on the surface, with anodic Mg dissolution in the α phase and the cathodic reaction primarily in the eutectic α-/β phase. The initiation in the larger grains could be explained by the smaller aluminum content in the larger grains due to the solidification process. Even though intermetallic Al–Mn particles show a high Volta potential difference with the connecting α phase, they are not involved in the initiation of the corrosion. This is explained by the position within the microstructure of Al–Mn particles embedded in the β phase and located away from the α phase.

Manuscript submitted May 7, 2007; revised manuscript received June 27, 2007. Available electronically September 20, 2007.

Magnesium alloys have low density and high specific strength, and these properties have created a great deal of interest in the use of these alloys in the motor and aerospace industries and in portable electronics. All of these industrial areas deal with applications in which weight is important. However, a big problem with magnesium alloys is their unsatisfactory corrosion properties. Understanding the corrosion properties of these alloys is vital if they are to become suitable alternatives for lightweight automotive components.

In recent years, significant improvements have been made in achieving better corrosion resistance, particularly by reducing the contents of impurities such as Fe, Cu, and Ni. Intermetallic phases, a result of the casting process, play an important role in the corrosion process. The role of these intermetallic phases has been addressed in a number of article.[1-6] However, despite the fact that magnesium alloys as structural materials are mostly used in atmospheric environments, the interpretation of the effect of microconstituents is almost exclusively based on electrochemical data obtained from measurement in solutions. The corrosion processes in aqueous solutions are different from those occurring in an atmospheric environment.

In an earlier work[7] the authors investigated the local nobility of the different intermetallic phases in the AZ91D alloy with the help of scanning Kelvin probe force microscopy (SKPFM). The results showed that under laboratory air conditions both the Al_8Mn_5 and the β-$Mg_{17}Al_{12}$ phases of the AZ91D alloy had a Volta potential which was, respectively, approximately 400 and 200 mV more noble than that of the α-magnesium phase. In the present work the influence of these intermetallic phases on the initial atmospheric corrosion process has been investigated further, using confocal laser scanning microscopy (CLSM) and SKPFM. Both SKPFM and CLSM are fairly new techniques in the field of corrosion. SKPFM can map the Volta potential with a lateral resolution in the nanometer range. This gives unique information on the local nobility of inhomogeneities on surfaces. The CLSM technique gives a three-dimensional image of the surface. In the materials science field the technique has mainly been used to investigate wear in the context of surfaces. A few studies have been made using CLSM in the corrosion science field.[8-11] The advantages of CLSM, compared to other profilemetry measurement techniques, are the short measurement times and the high magnification. High magnification can be achieved due to the short wavelength of the blue laser. The technique is described in detail in the literature.[12]

The purpose of the present work has been to better understand the influence of the microstructure on the initial steps of corrosion attacks on magnesium alloy AZ91D under atmospheric weathering conditions.

[z] E-mail: martin.jonsson@kimab.com

Experimental

Corrosion test panels of die cast AZ91D were supplied by Hydro Magnesium ASA Porsgrunn, Norway. The composition of the magnesium alloy is given in Table I.

The samples were machined to obtain small coupons (e.g., $45 \times 15 \times 3$ mm). The samples were sequentially polished and finally finished with 1 μm diamond paste. The polished samples were then ultrasonically cleaned in acetone and ethanol. In order to reveal their microstructure the samples were etched for 10 s in 1 mL HNO_3, 20 mL glacial acetic acid, 50 mL ethylene glycol and 17 mL distilled H_2O.[13] A part of the magnesium samples were contaminated with 1 $\mu g/cm^2$ NaCl, while the other samples were not contaminated. The samples were then exposed to 95% relative humidity in a closed vessel, where a saturated solution of K_2SO_4 was used to control the relative humidity.[14] After exposure the samples were pickled for 10 s in a solution of 200 g/L chromium trioxide (CrO_3) and 10 g/L silver nitrate ($AgNO_3$), then rinsed with water and ethanol and finally dried.

The confocal microscope model used in this experiment was LEXT OLS3000, supplied by Olympus. The light source in that instrument is a blue laser with a wavelength of 408 nm. Two scanning electron microscopes (SEMs) were also used. Element and line analysis was performed using a SEM model JSM6400 (ASEM), equipped with both an energy dispersive spectrometer (EDS) and a wavelength dispersive spectrometer. The acceleration voltage was set at 15 keV. The samples exposed to the confocal analysis were, before exposure to the humid air, examined with the use of a field emission gun scanning electron microscope (SEM), model LEO 1530, equipped with energy dispersive spectrometry (EDS), model INCA-energy, from LINK. The acceleration voltage was set at 15 kV. For the SKPFM measurements of the Volta potential a commercial atomic force microscope (Autoprobe M5) was used. The tip (Ultralever ULCT-AUHW) was made of silicon nitride coated with silver and supplied by ThermoMicroscopes (now: Veeco Instruments). All measurements were conducted at room temperature and at a controlled relative humidity (e.g., 40%). The Auger electron spectroscopy (AES) measurements were conducted on a Micro-Lab 310F instrument supplied by Termo VG Scientific. The base pressure was in the 1×10^{-10} range. The primary electrons had an energy of 15 keV. The Ar-ion sputtering was performed at an energy of 3 keV.

Table I. Nominal composition (wt %) of AZ91D magnesium alloy.

	Al	Zn	Mn	Si	Ni	Cu	Fe	ppm Be	Mg
AZ91D	9	0,79	0,23	0,02	0,0007	0,0027	0,0014	5	Remainder

Results

Microstructure.— The two SEM microscopes were used to identify interesting areas in the microstructure of the magnesium alloy AZ91D. A number of areas with intermetallic Al–Mn phases were imaged by the SEMs and the different intermetallic phases were identified using the EDS capability. In Fig. 1 the microstructure of the AZ91D alloy can be seen. The AZ91D has a microstructure typically consisting of a matrix of primary α phase grains with the β phase ($Mg_{17}Al_{12}$) surrounding the α phase grains. The composition of the β phase was approximately 71 atom % Mg and 27 atom % Al. In between these two phases was a zone consisting of a eutectic mix of the α phase and the β phase. The aluminum content of the eutectic phase varies and has a higher aluminum content compared to that of the α phase. The width and the variation of the aluminum content of the eutectic zone are dependent on the solidification rate. The AZ91D alloy also contains intermetallic Al–Mn phases. These Al–Mn intermetallics are often of the type η-Al_8Mn_5.[7] A thorough analysis of the microstructure of the AZ91D alloy showed that the iron content in the Al–Mn phase varies from 0.2 to 2.8 atom %.[7]

Particles 1 and 2 in Fig. 1 contain 1.3% and 1% iron, respectively. The aluminum and manganese content is 51% and 35%, respectively, for particle 1 and 55% and 35%, respectively, for particle 2. A certain amount of Mg was detected as well, due to the fact that the magnesium matrix influences the EDS signal. Normalizing the Al and Mn values, the composition corresponded to the η-Al_8Mn_5 type. The β phase ($Mg_{17}Al_{12}$) can be seen as white areas in Fig. 1.

Composition measurements.— The EDS capability of SEM was used to investigate the difference in element composition in different parts of the grain (Fig. 2). Both the line analysis and the point analysis capabilities were utilized. The line analysis gives the magnesium and aluminum content in counts along a line. As a complement, point analysis of the element composition was made at different points along the same line. The areas measured are denoted lines 1–4 and shown in Fig. 2. The magnesium and aluminum contents connected to the lines are given in Fig. 3a, 4a, and 5a. As can be observed, the aluminum content increases from the middle of the grain to the grain boundary, where the highest aluminum content can be found. From line 1 (Fig. 3a) it can be seen that the aluminum content within a larger grain is low, i.e., around 5%. Close to the β phase, within 6 μm distance, the aluminum content increases from

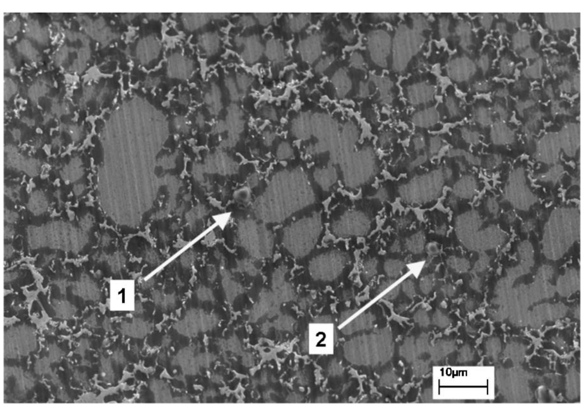

Figure 1. Microstructure of AZ91D magnesium alloy. Arrows 1 and 2 shows intermetallic particles of Al_8Mn_5 type. Particle 1 is composed of 1,3% Fe, 51% Al 35% Mn, particle 2 is composed of 1% Fe 55% Al, 35% Mn.

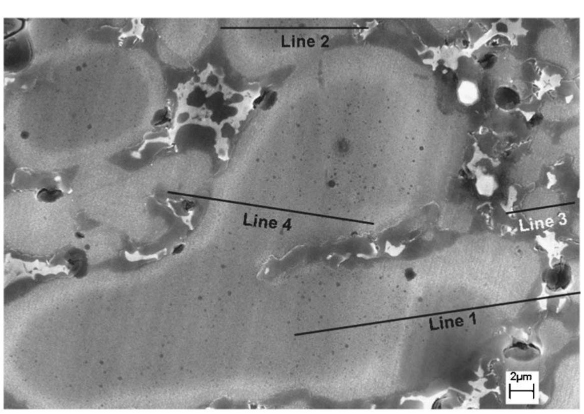

Figure 2. Grain from the AZ91D magnesium alloy. The magnesium and aluminum composition of lines 1–3 is given in Fig. 3a, 4a, and 5a.

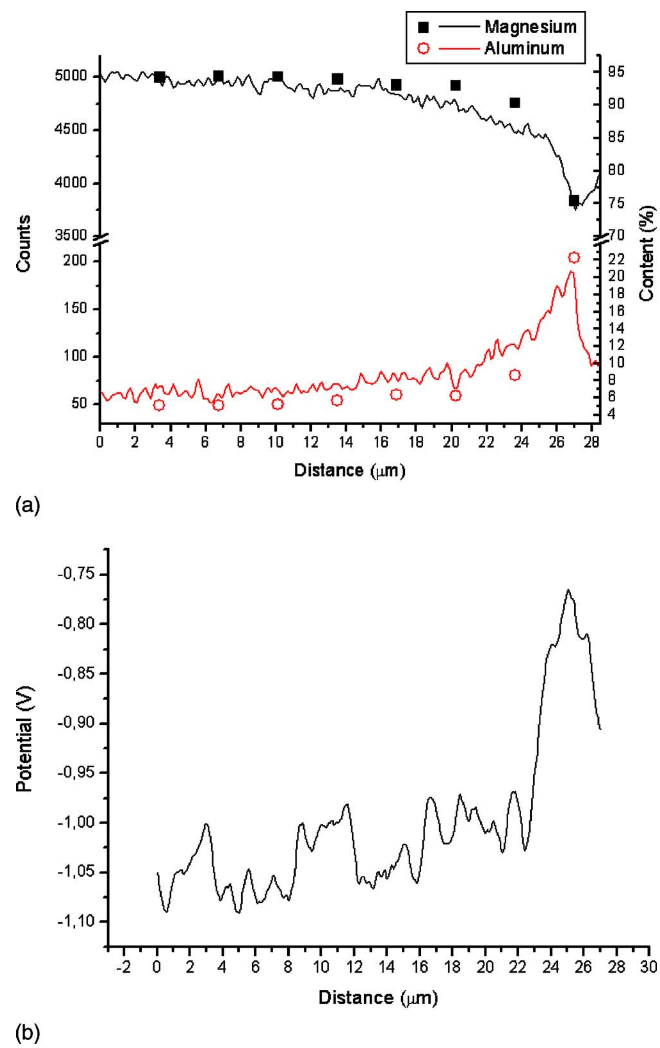

Figure 3. (Color online) (a) Magnesium and aluminum composition of line 1 in Fig. 2. (b) Volta potential distribution of line 1 in Fig. 6.

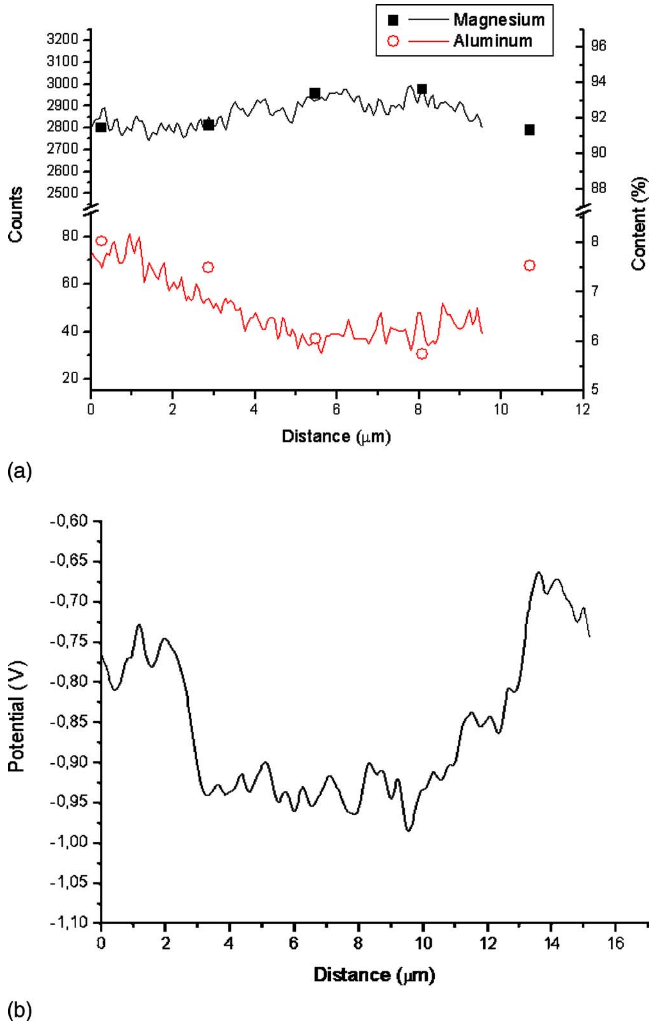

Figure 4. (Color online) (a) Magnesium and aluminum composition of line 2 in Fig. 2. (b) Volta potential distribution of line 2 in Fig. 6.

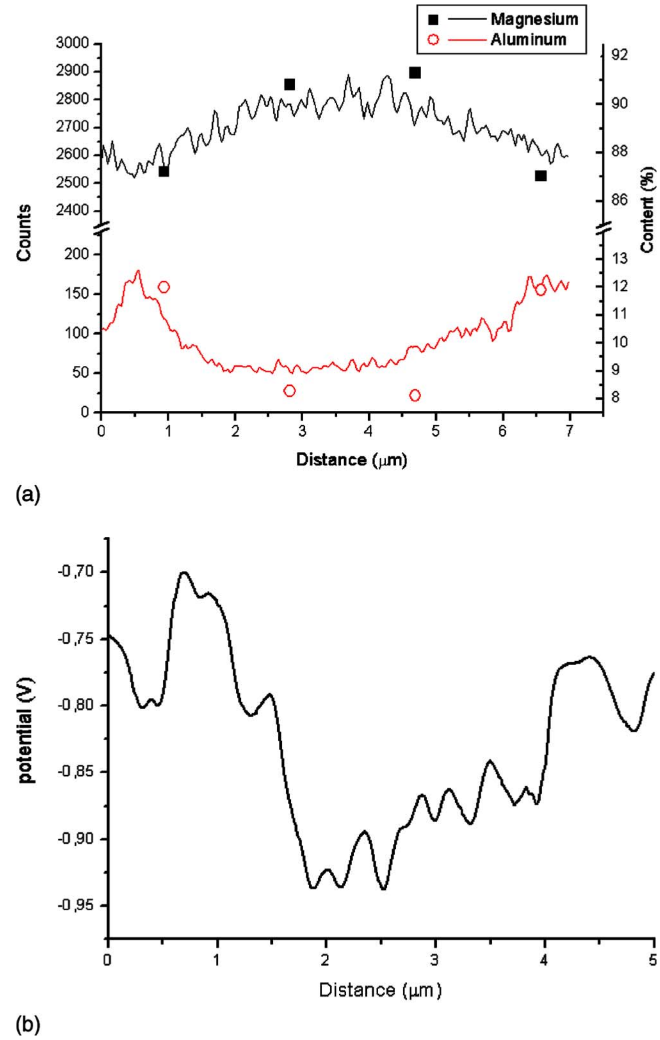

Figure 5. (Color online) (a) Magnesium and aluminum composition of line 3 in Fig. 2. (b) Volta potential distribution of line 3 in Fig. 6.

6% up to 23%. This area corresponds to the eutectic α-/β phase. In Fig. 2 the eutectic α-/β phase can be seen as darker areas surrounding the white β phase. It should be remembered that the EDS signal has an information depth that is dependent on the acceleration voltage, which is on the order of a few μm. The measurements are therefore not representative of the outermost layers of the surface. Figure 4a shows the aluminum content of a middle-sized grain. The aluminum content in the middle of the grain is around 6%. The smallest grain (Fig. 5a) has an aluminum content of around 8–9% in the middle of the grain, with an increase up to 11–12% at the boundaries. This is higher than the aluminum content in the larger grains.

Scanning Kelvin probe force microscopy measurements.— In order to understand the initial steps of the corrosion process the Volta potential of a magnesium grain was examined by means of SKPFM. The SKPFM instrument, which gives information on the local nobility of the microstructure in the alloy, was calibrated using bulk phases.[7] The Volta potential map in Fig. 6 shows the same part of the microstructure as the SEM image in Fig. 2. Comparing the EDS measurement from Fig. 3a, 4a, and 5a with the Volta potential measurement along the same lines (Fig. 3b and 5b), it can be seen that the Volta potential follows the aluminum content in the grains and that areas with a higher aluminum content give a higher Volta potential. An interesting observation is that a high Volta potential, around −750 mV, can be seen to the right in Fig. 3b as well as to the left in Fig. 4b, even though, according to the corresponding ele-

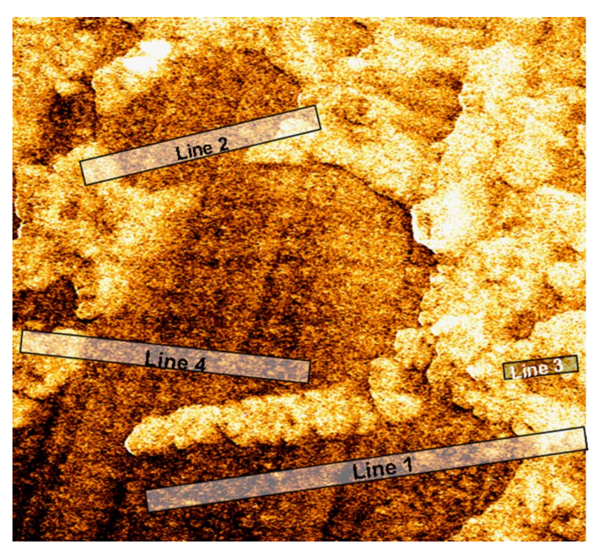

Figure 6. (Color online) Volta potential distribution of the same area seen in Fig. 2. The Volta potential of line 1–3 is given in Fig. 3b, 4b, and 5b.

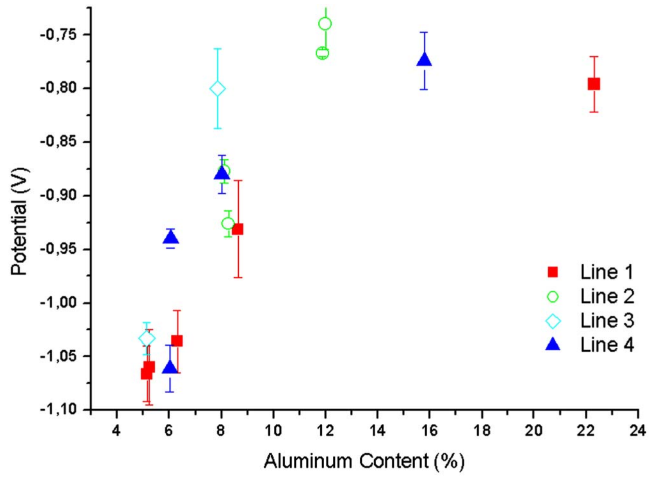

Figure 7. (Color online) Volta potential vs aluminum content of different points on lines 1–4.

ments analysis, the aluminum content is 22% and 12%, respectively, in the case of lines 1 and 2. The aluminum content taken from lines 1–4 in Fig. 2 is plotted in Fig. 7 against the Volta potential obtained from the corresponding points in Fig. 6. In the beginning the Volta potential increases linearly with the aluminum content. However, at an aluminum concentration of around 10% the Volta potential levels out at a potential of around −800 mV.

In Fig. 8 and 9 the Volta potential of ten different areas in the grain can be seen. The highest potential (−650 mV) was observed for area 10, which corresponds to the intermetallic Al–Mn particle. In areas 2, 4, 6 and 8, corresponding to the eutectic α-/β phase, the Volta potential ranges between −750 and −850 mV. The lowest potential (−1050 mV) within the investigated grain can be found for the α phase in area 1.

The difference in Volta potential between connecting areas can also be seen in Fig. 8 and 9. The highest potential difference (285 mV) can be found between the Al–Mn particle (area 10) and the surrounding α phase (area 9). An almost equally high difference (260 mV) occurs between the α phase in area 1 and the β phase in area 2. The smallest grain, area 3, has a potential difference of 120 mV between the grain and the surroundings. The slightly larger grain, area 7, has a potential difference of 160 mV in relation to the connecting area 8.

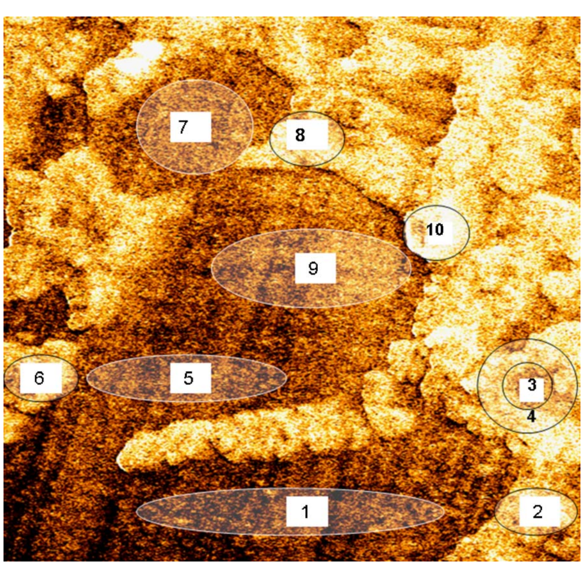

Figure 8. (Color online) Volta potential distribution of the same area seen in Fig. 2. The Volta potential of areas 1–10 is given in Fig. 9.

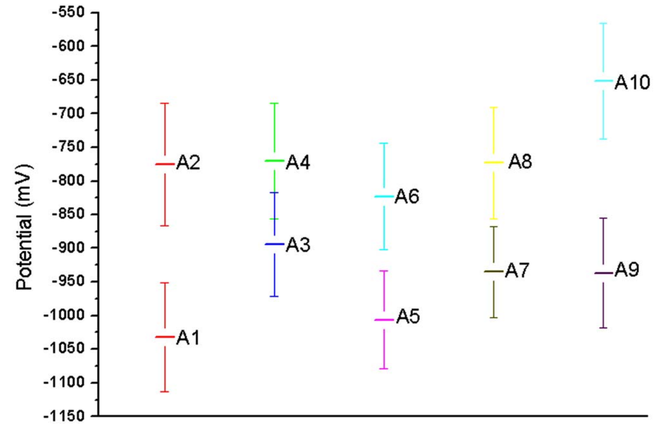

Figure 9. (Color online) Volta potential of areas 1–10 in Fig. 8.

Auger electron spectroscopy.— Since the composition of the outermost surface layers is of importance for the corrosion behavior of the magnesium alloy, Auger electron spectroscopy (AES) measurement was performed. The grain examined by means of AES can be seen in Fig. 10 and is the same grain that was examined using ASEM and SKPFM (Fig. 2 and 6). The top layer of the surface contains high amounts of carbon and oxygen, but only the ratio between the aluminum and magnesium is considered here. The diagram from the AES measurements shows the depth profiles of the aluminum/magnesium ratio at three different points in the Mg grain (Fig. 11). The three points correspond to the points in line 1 in Fig. 2. Point 1 corresponds to the β phase. As shown, the ratio between aluminum and magnesium content is high, above 0.5. In other words the aluminum content in the top surface layer is higher than that in the bulk phase. After 250 s of Ar^+ milling the aluminum content decreases and the ratio reaches a constant value of around 0.25. At points 2 and 3 the aluminum content is also high after the first 200 s of Ar^+ milling. Point 2 corresponds to the eutectic α-/β phase and point 3 to the α phase. The aluminum content at these two points is lower in the top layer, compared to point 1, but it is clear that the aluminum content is higher in the outermost layers compared to the bulk material. Thus, the results of the AES measurements show that in the different phases there is an enrichment of Al in the oxide layer and that this enrichment decreases in the order β phase > eutectic α-/β phase > α phase.

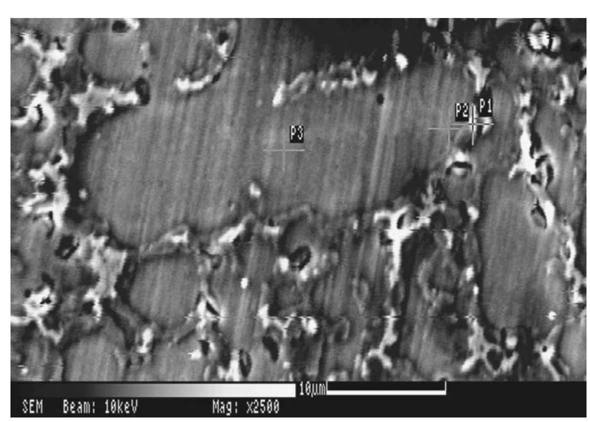

Figure 10. The same grain as seen in Fig. 2 and 6. Points 1–3 were examined using Auger electron spectroscopy and the results are shown in Fig. 11.

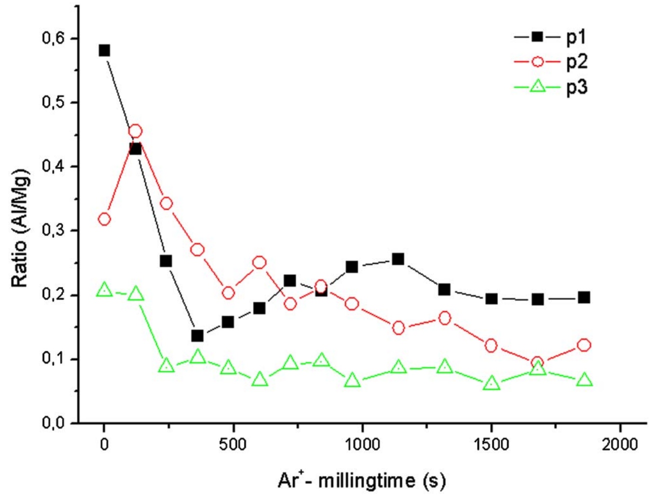

Figure 11. (Color online) Depth profiles of the aluminum/magnesium ratio of points 1–3 seen in Fig. 10 using Auger electron spectroscopy.

Confocal microscopy.— After the identification of different suitable areas with SEM (Fig. 1 and Fig. 12), the same areas were identified using confocal microscopy. The samples were then exposed to humid air 95% relative humidity (RH) for four days. Samples exposed with 1 $\mu g/cm^2$ NaCl were also investigated. Each day the identified areas were examined using confocal microscopy and the corrosion process was monitored. The corrosion products formed on magnesium alloy AZ91D under atmospheric conditions are mainly due to different magnesium carbonates such as hydromagnesite $[Mg_5(CO_3)_4(OH)_2 \cdot 4H_2O]$ and nesquehonite $(MgCO_3 \cdot 3H_2O)$.[15] These corrosion products are partly transparent for laser light. Therefore it is possible to monitor the development of a corrosion attack over time. Its development during 1–4 days can be seen in Fig. 13, which shows that corrosion can be observed already after one day of exposure. The attack starts at the boundary between the α phase and the eutectic α-/β phase. After two and three days of exposure the corrosion is more severe. Moreover, developing corrosion attacks can be seen to the right of the intermetallic Al–Mn particle. After four days of exposure the corrosion product has become so thick that the laser light cannot penetrate to the metal substrate. Hence, the thick corrosion product can be seen as a white area covering part of the grain.

After four days the corrosion products were pickled, revealing the corrosion attacks. Figures 14 and 15 show the pickled surface, and a SEM image of the same area can be seen in Fig. 12. As can be observed, the most severe corrosion attacks occurred in the largest α-Mg grain. The corrosion attack did not start around the Al–Mn phase, even though the largest potential difference could be found between the Al–Mn phase and the α phase. Instead the corrosion attack started at the boundary between the α phase and the eutectic α-/β phase. A line measurement in the confocal image (Fig. 15) shows that the trenches, formed at the boundary between the α phase and the eutectic α-/β phase, have a depth of approximately 1.3 μm. Eight different areas were examined. The same tendency could be seen in all these eight areas, with the initial corrosion attack starting in the largest grains at the boundary between the eutectic α-/β phase and the α phase, and not in the vicinity of the Al–Mn particle. The same results were obtained for the sample exposed to 1 $\mu g/cm^2$ NaCl.

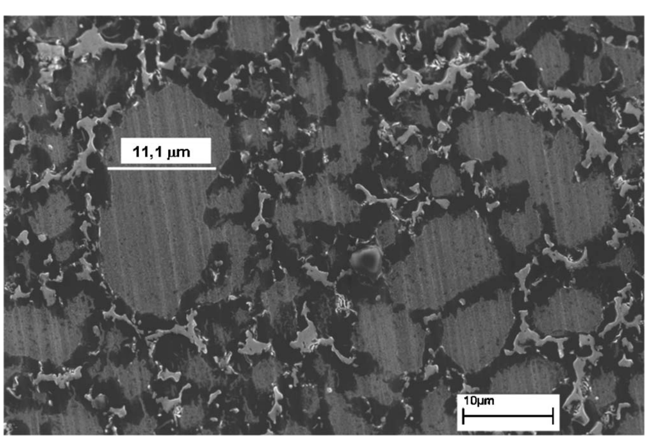

Figure 12. Part of Fig. 1 with a higher magnification.

Discussion

The results show that the corrosion attack was initiated in the larger grains and in the α phase in vicinity to the eutectic α/β phase, which has a higher aluminum content compared to the α phase. Furthermore, SKPFM measurements showed that the Volta potential varied for the different phases of the alloy and that the variation was related to the aluminum content of the different phases. The variation in the Volta potential, on the other hand, was linearly dependent on the aluminum content of the phases below 10% aluminum. Above that level, however, it was more or less constant. A similar behavior as regards the corrosion potential in solutions was observed by Mathieu et al.[6] However, the Volta potential should be dependent on the composition of the oxide rather than the bulk composition of the phases, and more surface specific Auger measurements indicated that the different phases of the oxide surface were enriched in Al. The content was higher in the phases with more Al in the bulk, indicating that the surface content of Al is related to the bulk content of this element. This has been shown in other investigations, and it has also been reported that in magnesium alloys, containing more than 4% aluminum, the alloy tends to form an oxide layer highly enriched in Al_2O_3.[16] It is suggested[17] that the aluminum concentration in the oxide layer is around 20% for alloys containing 5% Al and 8% Al, respectively, whereas a lower aluminum content of around 7% can be found for a Mg-2% Al alloy. According to Nordlien et al.[16] this explains the improved corrosion resistance found for Mg alloys that contain more than 4% Al. X-ray photoelectron spectroscopy measurements performed on Mg alloyed with Al show a significant enrichment of Al in the oxide up to a threshold value of about 35% wt % as the bulk Al content is increased above 4%.[17]

The aluminum content strongly influences the corrosion behavior of magnesium, as shown in several investigations.[3,15-18] Ambat[18] reports that the amount of aluminum needed for considerable protection is higher than 8%. However, it is also reported that in multiphase alloys a variation of the aluminum content within the microstructure leads to corrosion of regions where the aluminum content is lower than 8%. From the SEM analysis it is clear that the aluminum content in the different grains is dependent on the sizes of the grains. More accurately, the aluminum content in the grains is dependent on the cooling rate, and a high cooling rate results in small grains with a high aluminum content. In the same way the SKPFM measurement shows that the Volta potential for the same areas is also dependent on the grain size, the smallest grains giving the highest Volta potential and the largest grains the lowest Volta potential. This is related to the dependence of the Volta potential on the aluminum content as mentioned above.

As can be observed in Fig. 9, where potential differences between neighboring areas are shown, the highest voltage difference can be found for the couple between the Al–Mn phase and the α phase. Thus the driving force for corrosion between the Al–Mn phase and the α phase is high. However, the position of the Al–Mn particle in Fig. 12 is different. The particle is in this case imbedded in areas with a high aluminum content. It has been reported[19] that the majority of the Al–Mn particles that precipitate in Mg alloy

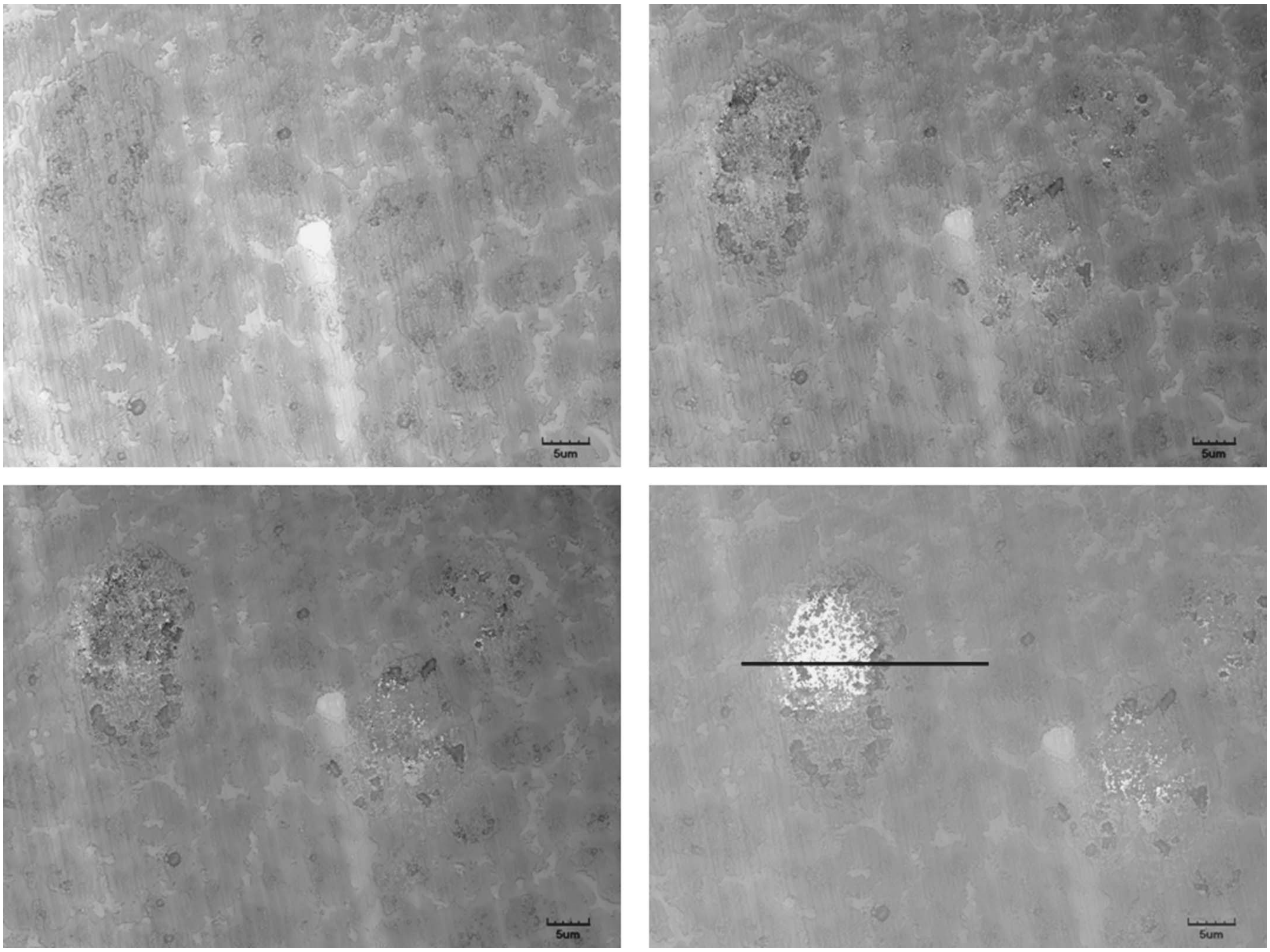

Figure 13. Confocal images showing the development of corrosion attack during 1–4 days exposure in 95% RH, top left: one day, top right: two days, bottom left: three days, bottom right: four days.

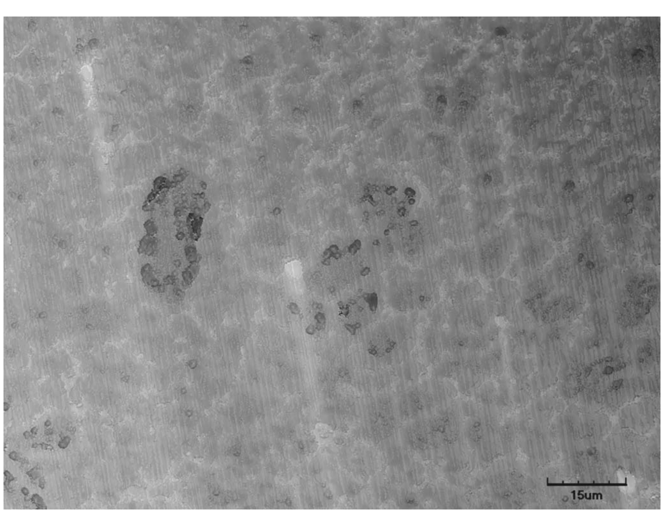

Figure 14. Confocal image over the same area as seen in Fig. 1. The area has been exposed for four days in 95% RH and the corrosion products have been removed through pickling.

AM50 can be found within the areas of a eutectic α-/β phase. This can be explained by the solidification process.[20] The first crystallized volumes, the α-Mg phase, had a reduced solute concentration of Mn, while the regions at the periphery contained a supersaturated solution of Mn and Al. Eventually the solute concentration in the remaining melt undergoes eutectic transformation forming a eutectic α-/β phase and the Al–Mn phases. Hence, the position, dimension and morphology of the eutectic α-/β phase and the η-Al_8Mn_5 phase were dependent on the processing parameters, especially the solidification rate. The same should also apply to the AZ91D alloy and variation in the microstructure has to be considered when interpreting the corrosion behavior of the alloy.

When the intermetallic Al–Mn phases are positioned within the eutectic α-/β phase or the β phase, galvanic coupling is possible between the eutectic α-/β phase and the intermetallic Al–Mn. However, due to the higher aluminum content in the eutectic α-/β phase the driving force is not strong enough for the initiation of corrosion attacks at these locations. Instead, as shown by the confocal microscope, the corrosion attacks start at the boundary between the α phase and the eutectic α-/β phase. As seen in Fig. 9, a high potential difference is also observed between the α phase in the larger grains (area A1) and the eutectic α-/β phase (area A2). Thus, a galvanic microelement was formed between these areas, with the cathodic reactions site located at the eutectic α-/β phase with an Al content of 10% or more, and at the β phase. However, it is possible that the

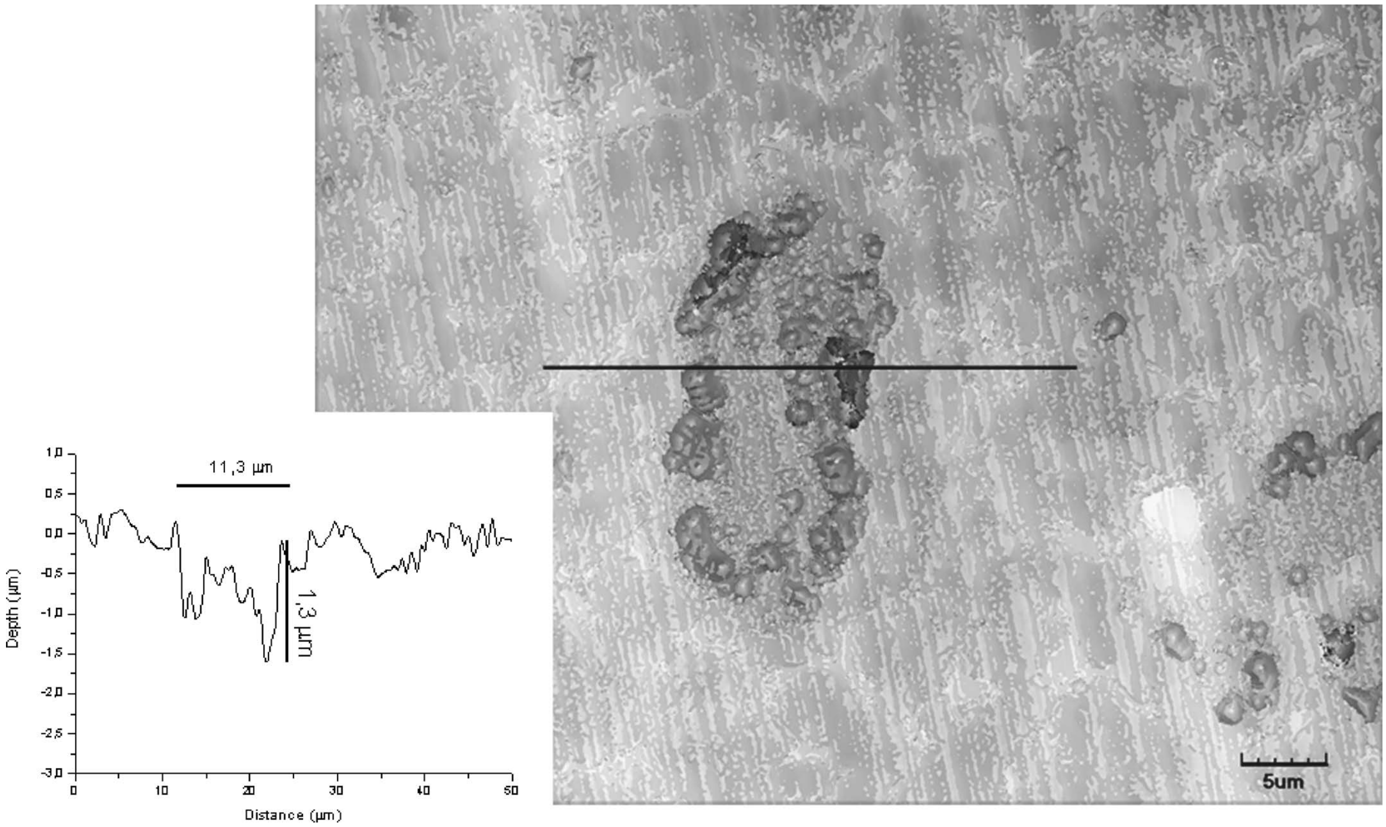

Figure 15. Confocal image over the grain seen in Fig. 12. The area has been exposed for four days in 95% RH and the corrosion products have been pickled. The depth and width of the black line is given in the diagram.

Al–Mn particles play a more important role in the initiation of the corrosion attacks if a thicker electrolyte layer is present on the surface or if a high Fe content in the Al–Mn particle makes it more efficient as a cathode. The electrolyte layer thickness is an important factor during atmospheric corrosion and it probably plays a very important role during the initiation of the atmospheric corrosion. When a clean metal surface is exposed to humid air, a thin absorbed water layer is formed with a thickness ranging from a few monolayers up to the order of ten layers,[21] depending on the humidity. In the presence of soluble compounds on the surface, thicker layers of water electrolyte form on the surface. Thus the formation of galvanic microelements with separated anodes and cathodes is dependent on the external conditions. Due to the low thickness of the water layer on the surface during atmospheric corrosion, especially in the absence of electrolyte forming species on the surface, the ohmic potential drop will be high. This is different from the case with corrosion in a bulk electrolyte, where the different phases are in connection through an electrolyte with higher conductivity. Thus, galvanic coupling between different constituents in the alloy is possible without any larger ohmic potential drop in the solution. By contrast, during atmospheric corrosion a larger ohmic potential drop in the thin water layer on the surface will decrease the possibility of galvanic coupling of alloy constituents located at larger distances from each other. Therefore it is likely that a galvanic couple is formed between the α phase in the larger grains and the eutectic α-/β phase. Further, the location of the β phase, further away from the α phase, causes a larger ohmic potential drop in the water layer. This makes it probable that the main part of the cathodic reaction takes place in the eutectic phase in the mediate vicinity of the α phase.

Conclusion

It has been shown that the microstructure is of vital importance for the initiation of atmospheric corrosion on the magnesium alloy AZ91D. The corrosion attack starts in the α phase in larger grains and is under atmospheric conditions initiated at the boundary between the α phase and the eutectic α-/β phase. The SKPFM measurement shows that a high Volta potential difference exists between the larger grains and the surrounding eutectic α-/β phase and/or β phase. A microgalvanic element is formed in the thin adlayer on the surface, with anodic Mg dissolution in the α phase and the cathodic reaction primarily in the eutectic α-/β phase. The Volta potential is also linearly correlated to the aluminum content in the bulk phases up to 8–10% aluminum. The initiation in the larger grains could be explained by the smaller aluminum content in the larger grains due to the solidification process which leads to a large Volta potential between the α phase in the larger grains and the eutectic phase (with Al content $>$8–10%). Even though intermetallic Al–Mn particles show a high Volta potential difference with the connecting α phase, they are not involved in the initiation of the corrosion. This is explained by the position within the microstructure of Al–Mn particles embedded in the β phase and thus located away from the α phase. This prevents the formation of a galvanic element with the Al–Mn particles as the cathode under atmospheric corrosion with very thin layers of water on the surface.

Corrosion and Metals Research Institute assisted in meeting the publication costs of this article.

References

1. O. Lunder, J. E. Lein, S. M. Hesjevik, T. K. Aune, and K. Nisancioglu, *Werkst. Korros.*, **45**, 331 (1994).

2. O. Lunder, J. E. Lein, T. K. Aune and K. Nisancioglu, *Corrosion (Houston)*, **45**, 741 (1989).
3. O. Lunder, J. H. Nordlien, and K. Nisangliou, *Corrosion Reviews*, **15**, 439 (1997).
4. O. Lunder, T. K. Aune, and K. Nisancioglu, *Corrosion (Houston)*, **43**, 291 (1987).
5. G. Song, A. Atrens, and M. Dargusch, *Corros. Sci.*, **41**, 249 (1999).
6. S. Mathieu, C. Rapin, J. Steinmetz, and P. Steinmetz, *Corros. Sci.*, **45**, 2741 (2003).
7. M. Jönsson, D. Thierry, and N. LeBozec, *Corros. Sci.*, **48**, 1193 (2006).
8. M. A. Alodan and W. H. Smyrl, *J. Electrochem. Soc.*, **144**, 282 (1997).
9. M. A. Alodan and W. H. Smyrl, *J. Electrochem. Soc.*, **145**, 1571 (1998).
10. G. O. Ilevbare, O. Schneider, R. G. Kelly, and J. R. Scully, *J. Electrochem. Soc.*, **151**, 453 (2004).
11. O. Schneider, G. O. Ilevbare, J. R. Scully, and R. G. Kelly, *Electrochem. Solid-State Lett.*, **4**, 35 (2001).
12. J. B. Pawley, *Handbook of Biological Confocal Microscopy*, Plenum, New York (1995).
13. K. J. Clark, *Metallography and Microstructures*, p. 425, American Society for Metals, Metals Park, OH (1985).
14. J. F. Young, *J. Appl. Chem.*, **17**, 241 (1967).
15. M. Jonsson, D. Persson, and D. Thierry, *Corros. Sci.*, **49**, 1540 (2007).
16. J. H. Nordlien, O. Sachiko, M. Noburo and K. Nisancioglu, *J. Electrochem. Soc.*, **143**, 2564 (1996).
17. J. H. Nordlien and K. Nisancioglu, Paper presented at European Symposium on Modification of Passive Films, Paris (1993).
18. R. Ambat, N. N. Aung, and W. Zhou, *Corros. Sci.*, **42**, 1433 (2000).
19. V. Y. Gertsman, J. Li, S. Xu, J. P. Thomson, and M. Sahoo, *Metall. Mater. Trans. A*, **36**, 1989 (2005).
20. C. J. Simensen, B. C. Oberlander, J. Svalestuen, and A. Thorvaldsen, *Z. Metallkd.*, **79**, 696 (1988).
21. P. Marcus, *Corrosion Mechanisms in Theory and Practice*, Marcel Dekker, New York (2002).